

IONIZED GAS IN DAMPED Ly α PROTOGALAXIES. I. MODEL-INDEPENDENT INFERENCES FROM KINEMATIC DATA

ARTHUR M. WOLFE¹

Department of Physics, and Center for Astrophysics and Space Sciences, University of California at San Diego, C-0424, La Jolla, CA 92093;
awolfe@ucsd.edu

AND

JASON X. PROCHASKA¹

The Observatories of the Carnegie Institute of Washington, 813 Santa Barbara Street, Pasadena, CA 91101; xavier@ociw.edu

Received 2000 May 30; accepted 2000 August 8

ABSTRACT

We investigate the kinematics of ionized and neutral gas in a sample of 35 damped Ly α systems (protogalaxies) using accurate quasar spectra obtained with HIRES, the echelle spectrograph on the Keck I 10 m telescope. Velocity profiles with resolution of $\sim 8 \text{ km s}^{-1}$ are obtained for high ions such as C IV and Si IV, and for intermediate ions such as Al III. Combining these profiles with similar quality profiles obtained previously for low ions such as Fe II, we investigate the kinematic state of damped Ly α protogalaxies in the redshift range $1.8 < z < 4.4$ by comparisons between data for various ion pairs. We find that the damped Ly α protogalaxies comprise distinct kinematic subsystems: a low-ion subsystem in which the low ions are physically associated with intermediate ions, and a high-ion subsystem containing neither low nor intermediate ions. The evidence for two subsystems stems from (1) differences between the widths of the velocity profiles, (2) misalignment in velocity space between the narrow components that make up the profiles in each subsystem, and (3) significant dissimilarities between the mean velocities of the high-ion and low-ion velocity profiles. In every case we find that test statistics such as velocity width and various asymmetry parameters distribute differently for low and high ions. We also find that the absence of intermediate and low ions from the high-ion subsystem indicates the latter is optically thin at the Lyman limit. Despite misalignment between their velocity components, the low- and high-ion kinematic subsystems are interrelated. This is indicated by detection of a statistically significant C IV versus low-ion cross-correlation function. It is also indicated by a systematic effect in which the C IV velocity widths are greater than or equal to the low-ion velocity widths in 29 out of 32 systems. These phenomena are consistent with the location of the two subsystems in the same potential well.

Subject headings: cosmology: theory — galaxies: evolution — quasars: general —
quasars: absorption lines

1. INTRODUCTION

For the past several years we have been studying the kinematics of gas in damped Ly α systems. We have focused on the *neutral* gas (Prochaska & Wolfe 1997, 1998; hereafter PW97, PW98) because of evidence suggesting that this is the source of baryons for stars in current galaxies (Wolfe 1995, 1997; Kauffmann 1996). We used the HIRES Echelle spectrograph (Vogt 1994) on the Keck I 10 m telescope to obtain accurate velocity profiles of low ions such as Fe II, Si II, Ni II, and Al II as they trace the kinematics of the neutral gas. The evidence for this is the large Al II/Al III ratios detected in most damped Ly α systems, which indicate that the singly ionized species are associated with neutral rather than ionized gas, provided that the ionizing radiation is supplied by external sources (Prochaska & Wolfe 1996).

The low-ion velocity profiles that we have measured comprise multiple narrow components that are not randomly distributed in velocity space. Rather, the strongest component tends to occur at the profile edge. In PW97 and PW98, we used these properties to test various models for damped Ly α systems. We adopted Monte Carlo techniques by sending random sight lines through gaseous configura-

tions specified by the cosmological model, the geometry and physics of the configuration, etc. We then computed distributions of test statistics such as the profile line widths and compared them with the empirical distributions. We first tested a simple model in which dark matter halos enclose *identical* randomly oriented exponential disks with rotation speeds $V_{\text{rot}} \approx 250 \text{ km s}^{-1}$ and exponential scale height $h \approx 0.3R_d$, where R_d is the radial scale length (PW97). We found this model to satisfy all the statistical tests. Its principal disadvantage, however, is that it is not set in a cosmological context. We then tested semianalytic versions of standard adiabatic cold dark matter cosmologies (SCDM) in which the neutral gas is confined to centrifugally supported disks in dark matter halos drawn from a computed mass function. The predominance of objects with low mass and low V_{rot} results in line widths that are too low to match the observed distribution, which extends to 300 km s^{-1} . In particular, the SCDM models considered by Kauffmann (1996) were found to be incompatible with the kinematic data. Furthermore, Jedamzik & Prochaska (1998) showed that no CDM cosmology is consistent with models that assume the damped Ly α systems to be single centrifugally supported disks within dark matter halos. On the other hand, Haehnelt, Steinmetz, & Rauch (1998) numerically simulated SCDM models with gas and dark matter, and found that at $z \sim 2$ the damped Ly α gas was distributed in low-mass protogalactic clumps rather than centrifugally

¹ Visiting Astronomer, W. M. Keck Telescope. The Keck Observatory is a joint facility of the University of California and the California Institute of Technology.

supported disks. The combination of infall and chaotic motions apparently reproduce the kinematic data.

This paper focuses on the kinematics of the *ionized* gas. Our aim is to place further constraints on galaxy formation models by studying gas located outside the neutral zones giving rise to damped Ly α lines. Ionized gas is a generic feature of such models, because initially the baryons are heated and ionized as they virialize in the potential wells of dark matter protogalactic halos. However, the indicated velocity field is not unique, with some models predicting radial collapse to neutral disks (Mo & Miralda-Escudé 1996), while others envision chaotic motions of ionized and neutral blobs (Haehnelt et al. 1998). As a result, determining the velocity structure of the ionized gas should help to clarify crucial events in the galaxy formation process (see accompanying paper, Wolfe & Prochaska 2000, hereafter Paper II).

In order to trace the velocity structure of the ionized gas, we used HIRES to obtain accurate velocity profiles of the C IV, Si IV, and Al III ions; these are shown in § 2. Through-

out this paper we assume the C IV ion to represent the highly ionized gas, since we have a larger number of accurate C IV than Si IV velocity profiles. In § 3 we construct frequency distributions of the profile line width, Δv , for each ion. We compare these with each other and with the Δv distribution for low ions such as Fe II or Si II, which presumably trace the kinematics of the neutral gas. To further compare the low-ion and high-ion gas, we examine correlations between the kinematics of low ions and high ions. To that end, we consider the difference between the means of low-ion and C IV profiles. We also consider the ratios of the Δv 's for various ion pairs. We then cross-correlate the velocity profiles of various ionic pairs. In § 4 we present model-independent conclusions following from our results.

2. DATA: OBSERVED VELOCITY PROFILES

Table 1 lists the sample of damped Ly α systems for which we have obtained velocity profiles. The spectra were acquired with HIRES at a resolution with FWHM \approx 6–8 km s $^{-1}$ and were reduced according to procedures outlined

TABLE 1
IONIC TRANSITIONS IN DAMPED Ly α SYSTEMS

QSO	z_{abs}	TRANSITION				REFERENCE ^a
		C IV	Si IV	Al III	Low-Ion	
Q0100+1304.....	2.309	1548	1393	1854	Ni II 1741	W
Q0149+3335.....	2.14076	1548	1393	1854	Fe II 1608	W
Q0201+3634.....	2.4628	1550	1393	1862	Si II 1808	W
Q0216+0803 ^b	2.2930	1550	...	1862	Si II 1808	S
Q0347–3800.....	3.0247	1548	1393	...	Fe II 1608	W
Q0458–0203.....	2.03955	1854	Cr II 2056	W
Q0528–2505A ^c	2.14104	1550	Si II 1808	S
Q0841–0203A.....	2.37452	1548	...	1854	Ni II 1741	W
Q0841–0203B.....	2.47622	1548	1393	1854	Fe II 1608	W
Q0930+28.....	3.23525	1548	1393	...	Fe II 1608	S
Q0951–04A.....	3.85669	...	1393	...	Si II 1526	W
Q1055+46.....	3.3172	1548	Fe 1608	S
Q1104–18.....	1.66138	1550	...	1854	Si II 1808	S
Q1108-07.....	3.60762	1548	1402	...	Fe 1608	W
Q1202–0725.....	4.38285	1548	1393	...	Si II 1304	S
Q1215+3322.....	1.9991	1548	1393	1854	Si II 1808	W
Q1223+1753.....	2.46608	1550	1402	1862	Si II 1808	S
Q1331+1704 ^b	1.77636	1550	...	1854	Si II 1808	W
Q1425+6039.....	2.8268	1550	1402	...	Fe II 1608	S
Q1759+7500.....	2.6253	1550	...	1854	Si II 1808	W
Q1850+40.....	1.99016	1862	Zn II 2026	S
Q1946+7658A.....	1.7382	1548	...	1854	Si II 1808	S
Q1946+7658B.....	2.8443	1550	1402	...	Si II 1304	S
Q2206–1958A ^b	1.920	1548	...	1854	Ni II 1741	W
Q2206–1958B.....	2.07623	1550	1402	...	Al II 1670	W
Q2212–1626.....	3.6617	1548	1402	...	Si II 1304	S
Q2230+02.....	1.85854	1550	1402	1862	Si II 1808	W
Q2231–0015.....	2.06615	1548	1393	1854	Si II 1808	W+S
Q2233+13.....	3.14927	1548	1402	...	Fe II 1608	S
Q2237–0608.....	4.0803	1548	1393	...	Al II 1670	S
Q2343+12.....	2.42969	1550	1393	1854	Si II 1808	S
Q2344+12.....	2.53779	1548	1402	...	Al II 1670	S
Q2348–1400 ^b	2.2794	1548	1393	1862	Fe II 1608	W
Q2359–0203A ^b	2.09507	1550	...	1854	Si II 1808	W
Q2359–0203B.....	2.15393	1550	...	1862	Si II 1526	W

^a W: Data collected by the authors' group; S: Data kindly provided by W. L. W. Sargent and collaborators.

^b C IV profiles exhibit some saturation.

^c The $z = 2.811$ damped system toward Q0528–2505 was omitted because its redshift exceeds that of the background QSO with which it may be associated.

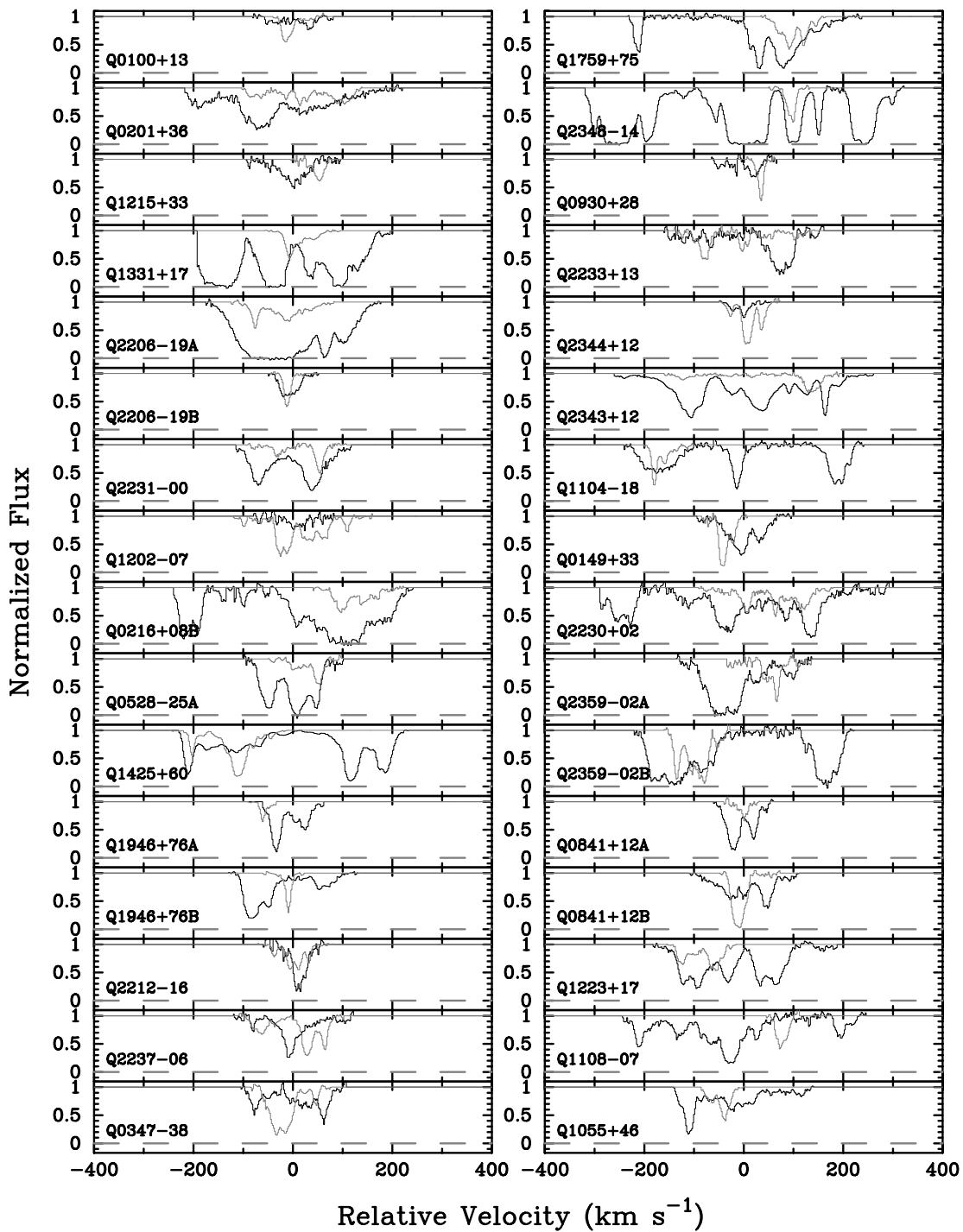


FIG. 1.—Velocity profiles of C IV (dark lines) and low-ion (gray lines) transitions for all damped $\text{Ly}\alpha$ protogalaxies in Table 1 in which HIRES C IV and low-ion profiles have been measured. The velocity $v = 0$ corresponds the absorption redshift, z_{abs} , shown in the table.

in PW97 and PW98. The coordinate name of the background QSO is given in column (1). Column (2) specifies the absorption redshift of the damped system. The entries in columns (3)–(5) contain the specific C IV, Si IV, and Al III transitions used in our analysis. Entries with ellipsis dots indicate that statistically significant profiles were not observed. Column (6) lists the low-ion transitions used in our analysis, and column (7) gives the data references. Here and throughout the paper, the term “low ion” refers to ions such as Fe II and Si II, the dominant ionization states in neutral gas with large optical depths at the Lyman limit, i.e.,

$\tau_{\text{LL}} > 10^4$. The ionization potential (IP) of such ions is greater than 1 ryd, i.e., 13.6 eV, while the IP of the next lower state (typically the neutral atom, except for O) is less than 1 ryd. The term “high ion” refers to ions in which the next lower state has IP $\gg 1$ ryd, for example Si IV and C IV. Photoionization studies show these ions to be in gas that is optically thin at the Lyman limit or in gas with moderate Lyman-limit optical depths ($\tau_{\text{LL}} < 10^2$). Finally, we introduce the term “intermediate ions” to describe those ions in which the next lower ionization state has IP $\gtrsim 1$ ryd (e.g., Al III). The same photoionization studies show that at the

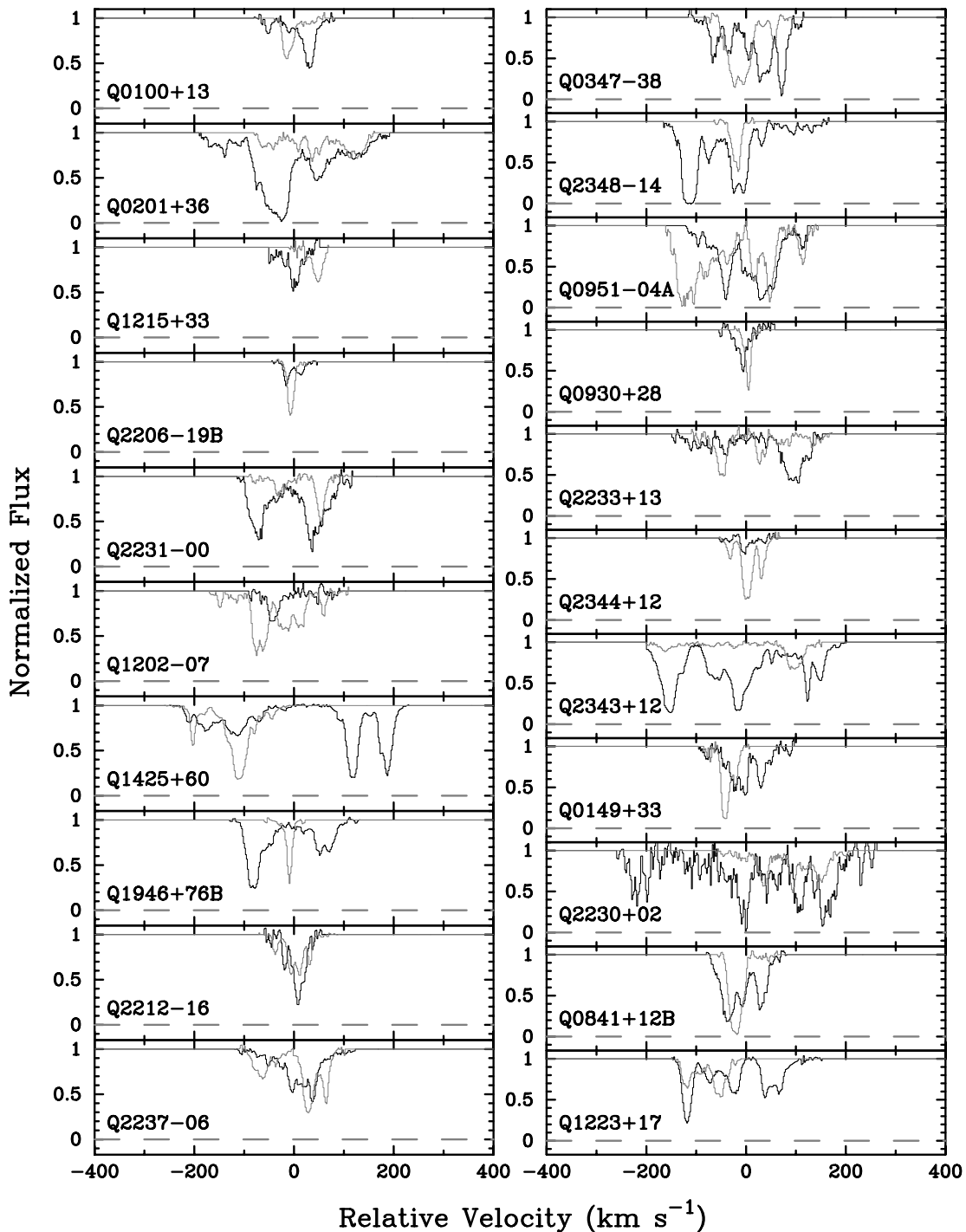


FIG. 2.—Velocity profiles of Si IV (*dark lines*) and low-ion (*gray lines*) transitions for all damped Ly α protogalaxies in Table 1 in which HIRES Si IV and low-ion profiles have been measured. Velocity scale same as in Fig. 1.

column densities required for detection (i.e., above 10^{14} cm^{-2}) these ions arise in gas that is optically thick at the Lyman limit. As a result, association of high ions with intermediate ions indicates that the gas is optically thick at the Lyman limit.

The velocity profiles are shown in Figures 1–5, which plot flux versus velocity, where the flux, $I(v)$, is normalized to unit continuum. In Figures 1–3, we compare C IV, Si IV, and Al III with the corresponding low-ion profiles. The dark curves depict the high and intermediate ions, and the gray

curves depict the low ions. Figure 4 compares the C IV (*dark curves*) and Si IV (*gray curves*) profiles, and Figure 5 compares C IV (*dark curves*), Al III (*light gray curves*), and the low ions (*medium gray curves*). In all cases, $v = 0$ km s^{-1} corresponds to the redshifts in Table 1. The low-ion transitions were selected on the basis of criteria outlined in PW97 and PW98; i.e., for high signal-to-noise ratios and absence of saturation. The high-ion transitions were selected according to the same criteria, where possible. In some cases, the only transitions available exhibit saturation over sizable veloc-

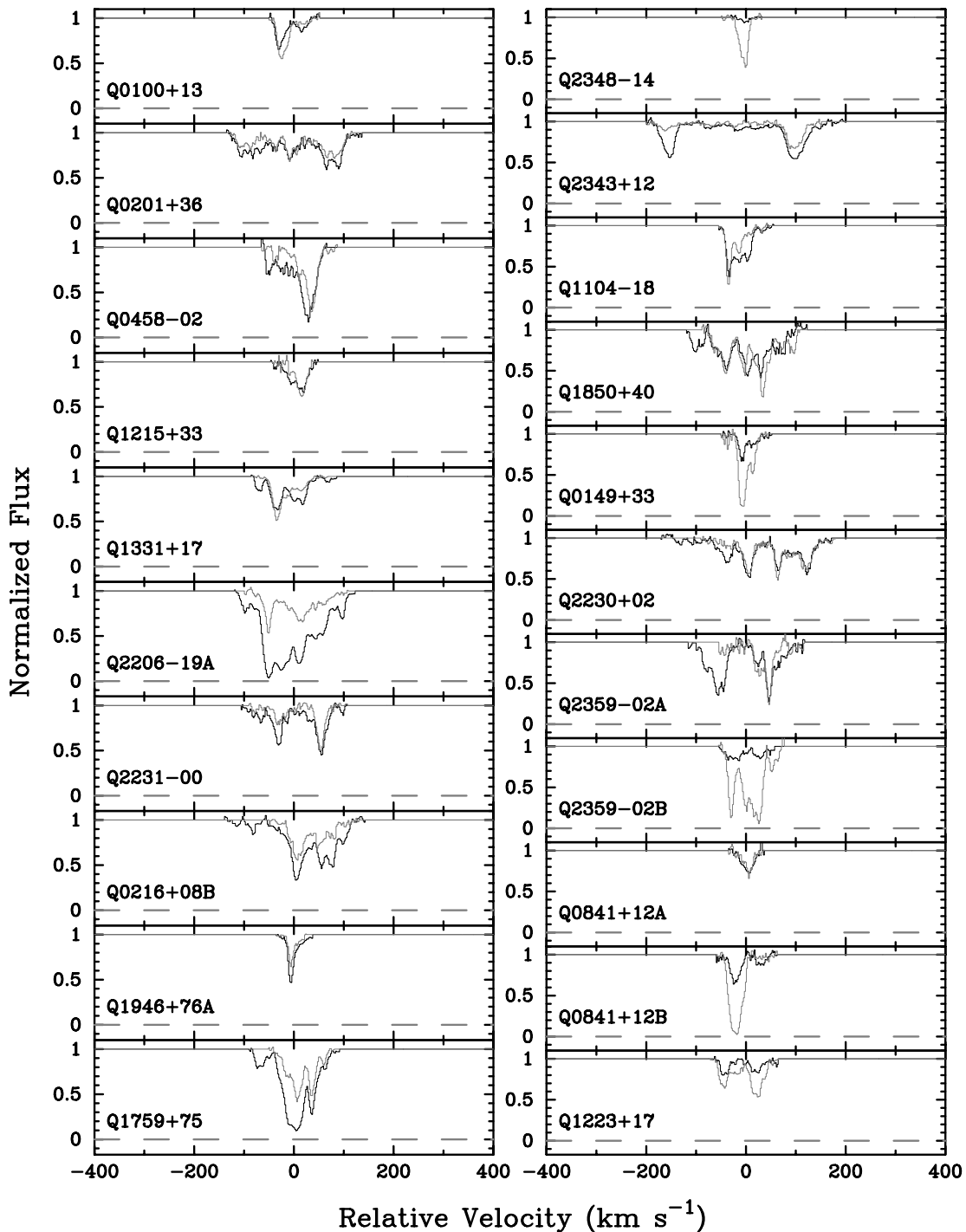


FIG. 3.—Velocity profiles of Al III (dark lines) and low-ion (gray lines) transitions for all damped $\text{Ly}\alpha$ protogalaxies in Table 1 in which HIRES Al III and low-ion profiles have been measured. Velocity scale same as in Fig. 1.

ity intervals. The C IV profiles toward Q0216+08B, Q1331+17, Q2206-19A, Q2348-14, and Q2359-02A contain significant regions in velocity space with strong saturation. The same is true for the Si IV profile toward Q2348-14. As emphasized in PW97, some of the statistical tests used to compare the data with model predictions are sensitive to saturation; in particular, determination of test statistics measuring the profile asymmetries can be inaccurate in the presence of saturation. However, the results of statistical tests described below did not change qualitatively when the saturated C IV profiles were excluded from the

sample. As a result, the saturated profiles will be included in all subsequent analysis.

The velocity profiles leave the following impressions:

1. In common with the low-ion profiles, the intermediate- and high-ion profiles exhibit a multicomponent structure comprising several narrow components spanning a wide range of velocity intervals.

2. The C IV and low-ion profiles in Figure 1 are kinematically disjoint. In many cases, strong C IV absorption components are at velocities at which low-ion absorption is

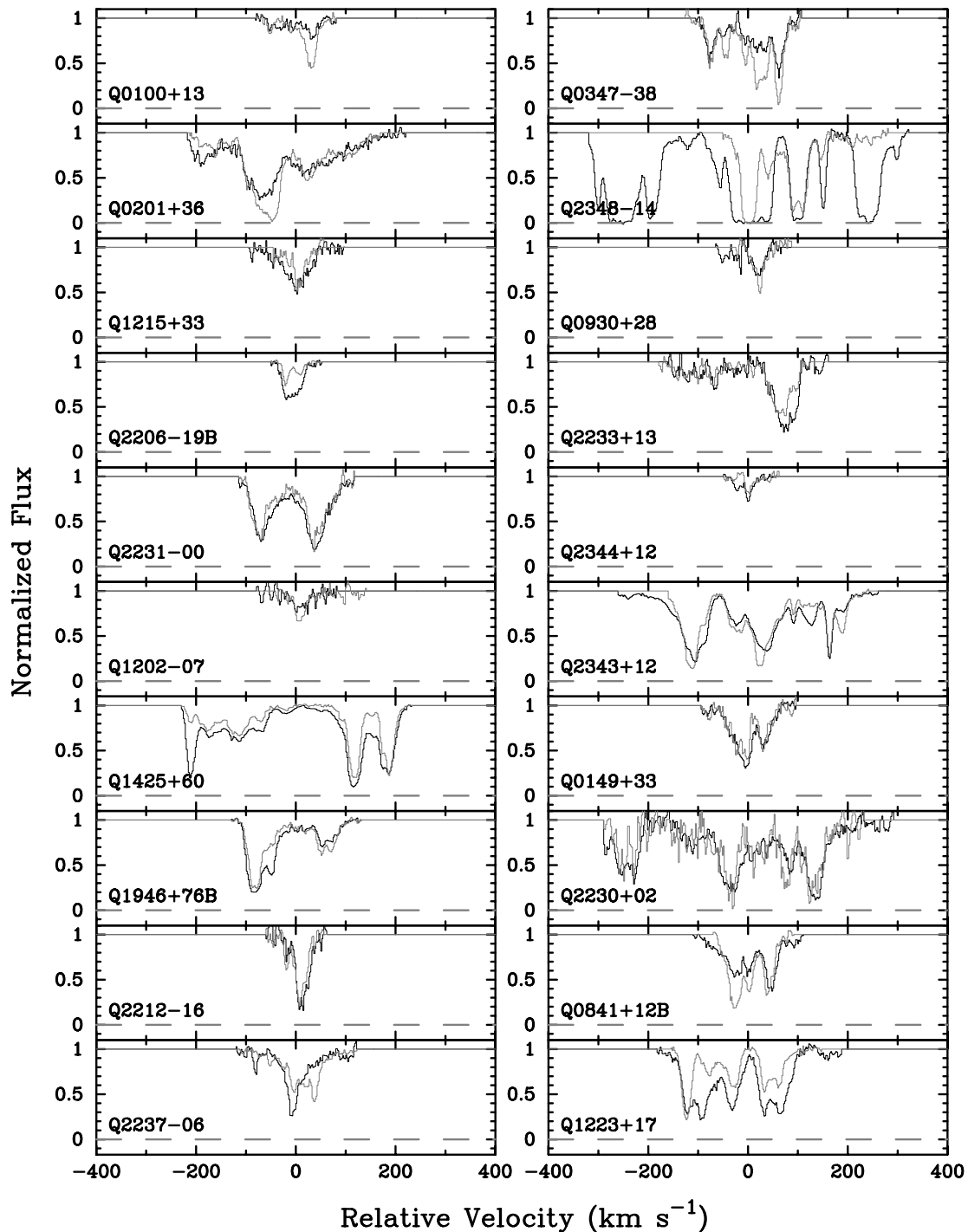


FIG. 4.—Velocity profiles of C IV (*dark lines*) and Si IV (*gray lines*) transitions for all damped Ly α protogalaxies in Table 1 in which HIRES Si IV and C IV profiles have been measured. Velocity scale same as in Fig. 1.

weak or absent. In other cases, C IV absorption is weak or absent at velocities at which low-ion absorption is strong. In many cases, the velocity centroids of the C IV and low-ion profiles appear to be significantly different.

3. Despite their differences, the C IV and low-ion velocity profiles overlap in velocity space in such a way that the low-ion profiles generally lie within the high-ion profiles.

4. The low-ion profiles also appear to be kinematically disjoined from the Si IV profiles (see Fig. 2).

5. The Al III and low-ion profiles appear to be strongly correlated (Fig. 3).

6. The C IV and Si IV profiles appear to be strongly correlated (Fig. 4).

7. In many cases, C IV absorption occurs in regions of velocity space that are free of Al III and low-ion absorption (Fig. 5).

8. In most cases, the velocity widths of C IV and Si IV velocity profiles exceed the velocity widths of the Al III and low-ion profiles.

9. Although the low-ion and high-ion velocity profiles exhibit “edge-leading” asymmetries, in which the strongest velocity components are at the profile edges, the high ions

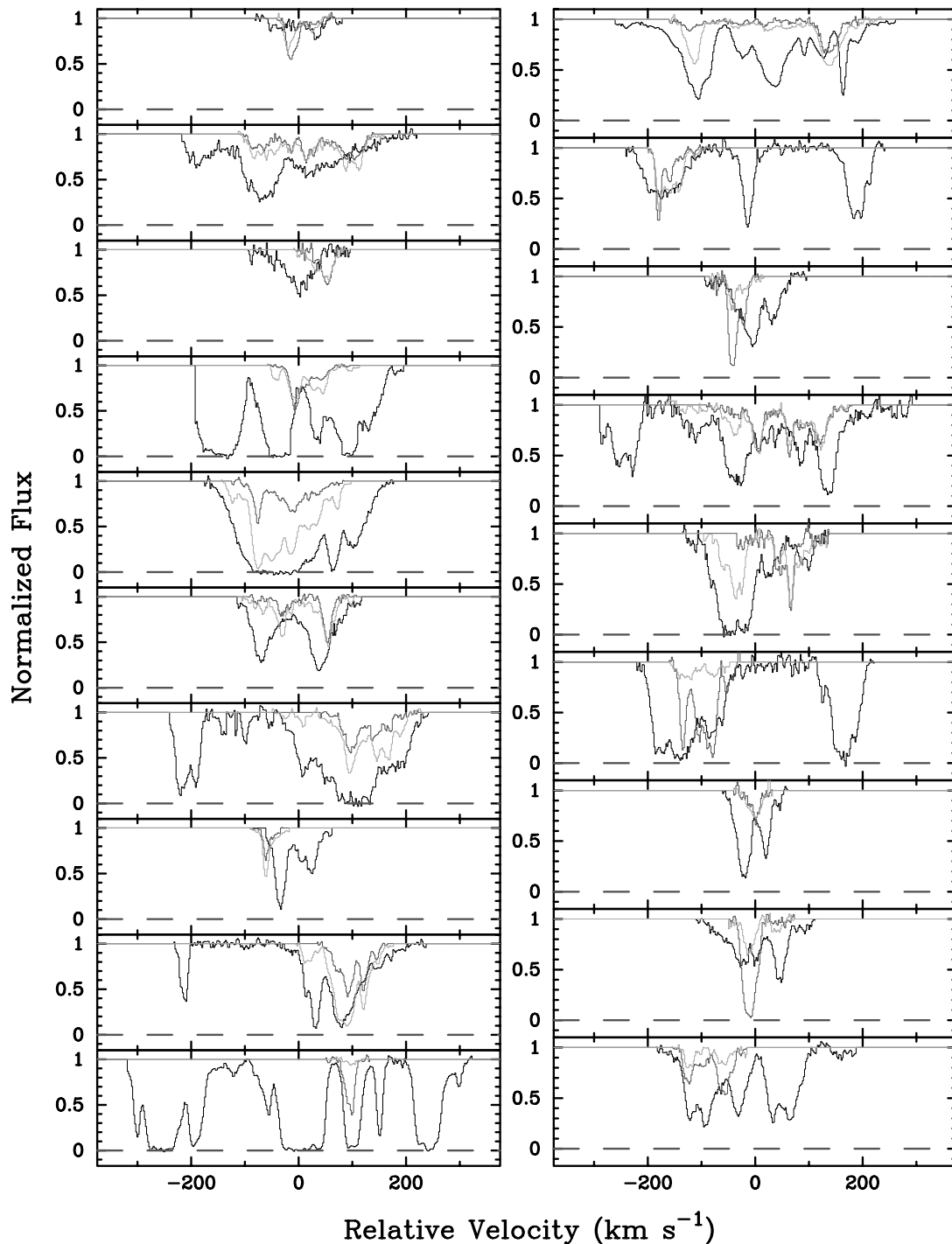


FIG. 5.—Velocity profiles of C IV (dark lines), Al III (light gray lines), and low-ion (medium gray lines) transitions for all damped $\text{Ly}\alpha$ protogalaxies in Table 1 in which Al III, C IV, and low-ion profiles have been measured. Velocity scale same as in Fig. 1.

tend to exhibit peaks at both edges more often than the low ions.

In the sections that follow, we introduce several tests to quantify these phenomena.

3. TEST STATISTICS

3.1. Distributions for Single Ions

To describe the kinematics of the gas in a quantitative manner, we consider test statistics that characterize the extent and shape of the velocity profiles. We discuss dis-

tributions of such statistics drawn from the profiles corresponding to given ions and then compare them. These empirical distributions are used to test theoretical models in Paper II.

In PW97 we characterized the extent and asymmetry of the velocity profiles with four test statistics. Briefly stated, they are:

1. Δv , the velocity interval enclosing the central 90% of the integrated optical depth, $\int \tau(v)dv$, where $\tau(v) \equiv \ln[1/I(v)]$.
2. f_{mm} , the “mean-median statistic” given by $|v_{\text{median}}$

– $v_{\text{mean}}|/(\Delta v/2)$, where v_{median} and v_{mean} are the median and mean velocities of the profiles.

3. f_{edg} , the “edge statistic” given by $|v_{\text{peak}} - v_{\text{mean}}|/(\Delta v/2)$, where v_{peak} is the velocity of the absorption component with peak optical depth.

4. f_{tpk} , the “two-peak statistic” given by $\pm |v_{\text{tpk}} - v_{\text{mean}}|/(\Delta v/2)$, where v_{tpk} is the velocity of the component with second-strongest peak optical depth: f_{tpk} is

positive if $v_{\text{peak}} < v_{\text{tpk}} < v_{\text{mean}}$ and negative if $0 < v_{\text{tpk}} < v_{\text{peak}}$ or $v_{\text{tpk}} > v_{\text{mean}}$. If necessary, the optical depth profiles have been reflected in velocity space in such a way that v_{peak} is always located at $v \leq v_{\text{mean}}$.

Distributions for each test statistic are illustrated in Figure 6 for the low-ion, Al III, Si IV, and C IV transitions. In PW97 and PW98 we focused on the low-ion distributions.

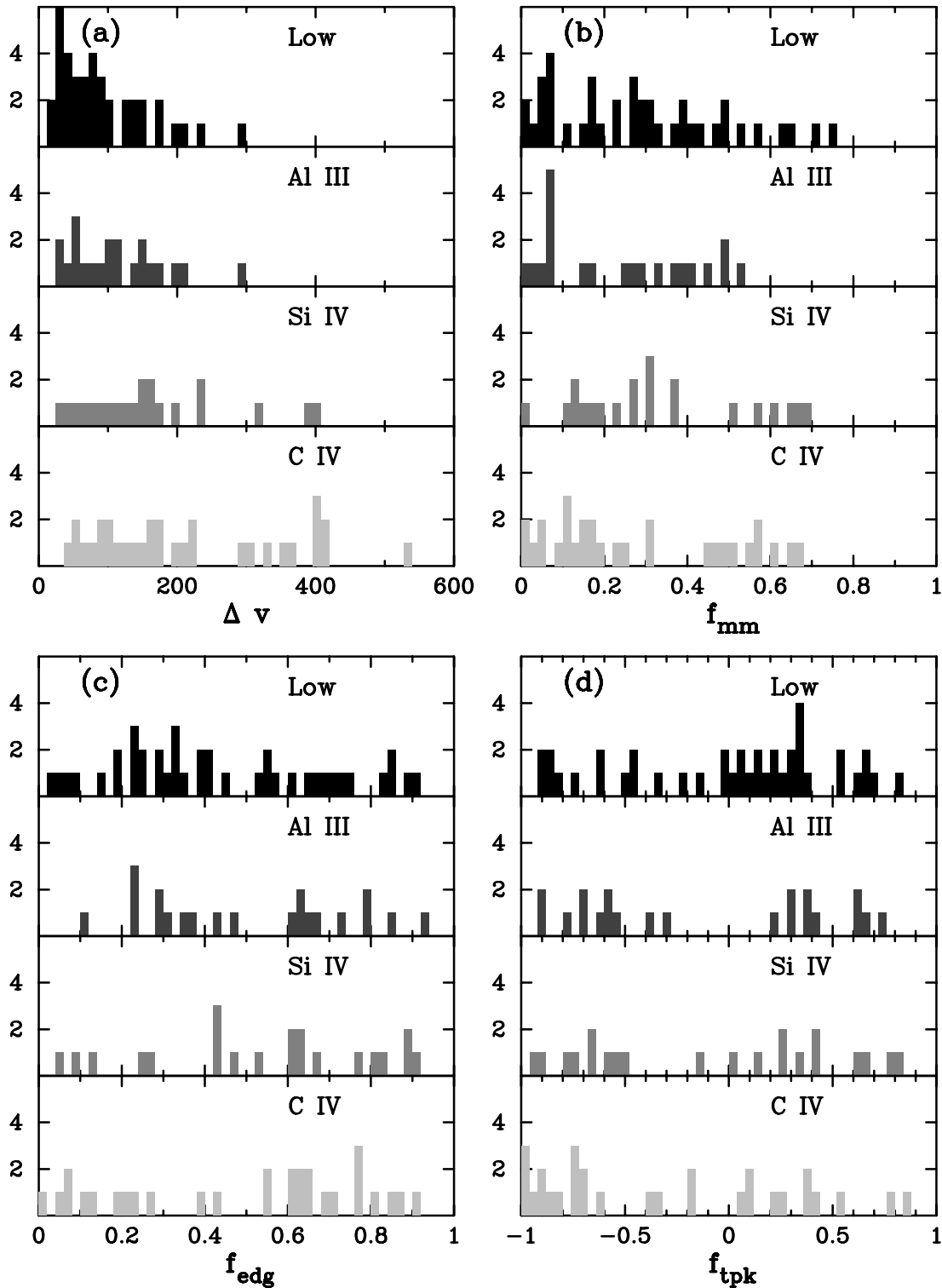


FIG. 6.—Empirical distributions of test statistics (a) Δv , (b) f_{mm} , (c) f_{edg} , and (d) f_{tpk} for low-ion, Al III, Si IV, and C IV velocity profiles

We used them to argue in favor of models in which the low ions were confined to rapidly rotating disks (rotation speeds $\approx 250 \text{ km s}^{-1}$) and to rule out several other models. We return to this topic in Paper II. Here we check the null hypothesis that low-ion and high-ion kinematics stem from the same process. We do this by computing P_{KS} , the Kolmogorov-Smirnov probability that each high-ion or intermediate-ion test statistic is drawn from the same parent population as the corresponding low-ion statistic. Figure 6 shows that the null hypothesis cannot be dismissed, with two exceptions. First, the null hypothesis is highly unlikely when comparing low-ion versus C IV distributions of Δv , since $P_{\text{KS}}(\Delta v) = 0.002$, and when comparing low-ion versus Si IV distribution of Δv , since $P_{\text{KS}}(\Delta v) = 0.021$: the high ions do not exhibit as much power at low Δv as the low ions, and they exhibit more power than the low ions at $\Delta v > 200 \text{ km s}^{-1}$. Indeed, the low probabilities suggest that the low and high ions are in two distinct kinematic subsystems. Second, the null hypothesis is unlikely in the case of low-ion versus C IV distributions of f_{tpk} because $P_{\text{KS}}(f_{\text{tpk}}) = 0.035$; i.e., the C IV profiles display more double-peaked profiles than the low ions. On the other hand, $P_{\text{KS}}(f_{\text{tpk}}) = 0.23$ in the case of low-ion versus Si IV profiles. Since compatibility of the Si IV and low-ion distributions of f_{tpk} cannot not be ruled out, this is the only case in which the C IV and Si IV kinematics differ. We suspect that statistics of small numbers may be affecting the Si IV distribution, a possibility we will test when larger samples become available.

3.2. Correlations between Macroscopic Kinematic Properties of Ion Pairs

We now turn to correlations between kinematic properties of gas in different ionization states. First we consider distributions of the following new test statistic:

5. $\delta v = v_{\text{mean}}(\text{ion } a) - v_{\text{mean}}(\text{ion } b)$, i.e., the difference between the means of the velocity profiles of ion a and ion b .

Figure 7a shows the distribution of δv when a and b are (1) low-ion and C IV, (2) C IV and Al III, (3) C IV and Si IV, and (4) low-ion and Al III. Not surprisingly, the distribution widths are narrower for C IV versus Si IV and low-ion versus Al III than for low-ion versus C IV. This just indicates that the high-ion subsystem includes the high ions C IV and Si IV, but not the intermediate Al III ions, which are mainly associated with the low-ion subsystem. The standard deviations for the three distributions are given in Table 2. Although the dispersion of the low-ion versus C IV distribution is relatively high, $\sigma_\delta = 67 \text{ km s}^{-1}$, it is sufficiently low to place crucial restrictions on most models (see Paper II).

Next we consider correlations between the Δv of various ion pairs. In Figure 8a we plot $\Delta v_{\text{C IV}}$, the Δv inferred from the C IV profiles, versus Δv_{low} , the Δv inferred from the

low-ion profiles. In Figures 8b and 8c we do the same for $\Delta v_{\text{C IV}}$ versus $\Delta v_{\text{Si IV}}$, the velocity width of Si IV, and $\Delta v_{\text{Al III}}$, the velocity width of Al III, versus Δv_{low} . The figure shows $\Delta v_{\text{C IV}}$ to be correlated with $\Delta v_{\text{Si IV}}$, and $\Delta v_{\text{Al III}}$ with Δv_{low} . This is demonstrated in Table 3, showing the Kendall τ correlation coefficients. The only cases with statistically significant τ (i.e., at the 5σ level) are for the C IV versus Si IV correlation and the Al III versus low-ion correlation. We conclude that statistically significant correlations exist between $\Delta v_{\text{C IV}}$ and $\Delta v_{\text{Si IV}}$, and between $\Delta v_{\text{Al III}}$ and Δv_{low} . Evidence for such correlations within the remaining ion pairs is marginal. On the other hand, Figure 8a shows that for all but three objects $\Delta v_{\text{C IV}} \geq \Delta v_{\text{low}}$, and even the three exceptions nearly satisfy this relation. In other words, the low-ion velocity width acts as a “floor” to the high-ion velocity widths. While not a correlation, this is an important systematic effect, indicating that the high-ion and low-ion systems are interrelated in a way that must be accounted for by models of the ionized gas.

The relationship between the velocity widths is quantitatively described by the test statistic:

6. $f_{\text{ratio}} \equiv \Delta v_a / \Delta v_b$, the ratio of the velocity widths of ion a to those of ion b .

The corresponding distributions are shown in Figure 7b. Note how the f_{ratio} for low-ion versus C IV and C IV versus Al III are uniformly distributed at $0.7 \leq f_{\text{ratio}} \leq 3$, while the C IV versus Si IV and low-ion versus Al III distributions exhibit significant peaks at $f_{\text{ratio}} = 1$. This is further evidence for an association between Al III and low ions, and between C IV and Si IV.

We searched for evidence that other test statistics were correlated between the different ion pairs. None was found, with the possible exception of correlations between the Al III and low-ion f_{edg} , which exhibit Kendall τ coefficients at the 3.0σ level. Correlations between the C IV and Si IV f_{tpk} were found at the 2.5σ level. We also checked for correlations between pairs of test statistics corresponding to a given ion. Ledoux et al. (1998) reported evidence for a low-ion correlation between f_{edg} and Δv out to $\Delta v = 150 \text{ km s}^{-1}$, but found no such correlation at $\Delta v > 150 \text{ km s}^{-1}$. They claimed that the “break” at 150 km s^{-1} argued against the presence of damped Ly α systems comprising disks with rotation speeds greater than 150 km s^{-1} . It is difficult to assess the validity of their claim, since no quantitative estimate was given for the significance of the correlation. With our larger data set (39 versus their 26 systems), we find evidence for such a correlation at the 3.6σ level, but no convincing evidence for a “break” at $\Delta v \approx 150 \text{ km s}^{-1}$. In fact, when systems with $\Delta v > 150 \text{ km s}^{-1}$ were eliminated, the significance level of the correlation *decreased* to 2.8σ . This argues against the presence of such a “break” and is consistent with a correlation extending to $\Delta v \approx 250 \text{ km s}^{-1}$.

TABLE 2
DISPERSIONS OF δv DISTRIBUTIONS

Dispersion (km s^{-1})	C IV vs. Low-Ion	C IV vs. Si IV	Al III vs. Low-Ion
$\sigma_{\delta v}^a$	67.0 ± 8.2	23.2 ± 3.4	30.0 ± 4.2

^a 1σ in $\sigma_{\delta v}$ computed by assuming that $(n-1)s^2/\sigma^2$ is distributed as $\chi^2(n-1)$, where n is the number of degrees of freedom, $\chi^2(n-1)$ is χ^2 for $n-1$ degrees of freedom, and where s^2 and σ^2 are the measured and true variance of $\sigma_{\delta v}$, respectively (Frodesen, Skjeggstad, & Tofte 1979, p. 109.)

TABLE 3
CORRELATIONS BETWEEN IONIC VELOCITY INTERVALS

ION	KENDALL τ			
	C IV	Si IV	Al III	Low-Ion
C IV	0.80 ± 0.16	0.57 ± 0.16	0.33 ± 0.16
Si IV	0.76 ± 0.22	0.52 ± 0.15
Al III	0.73 ± 0.16

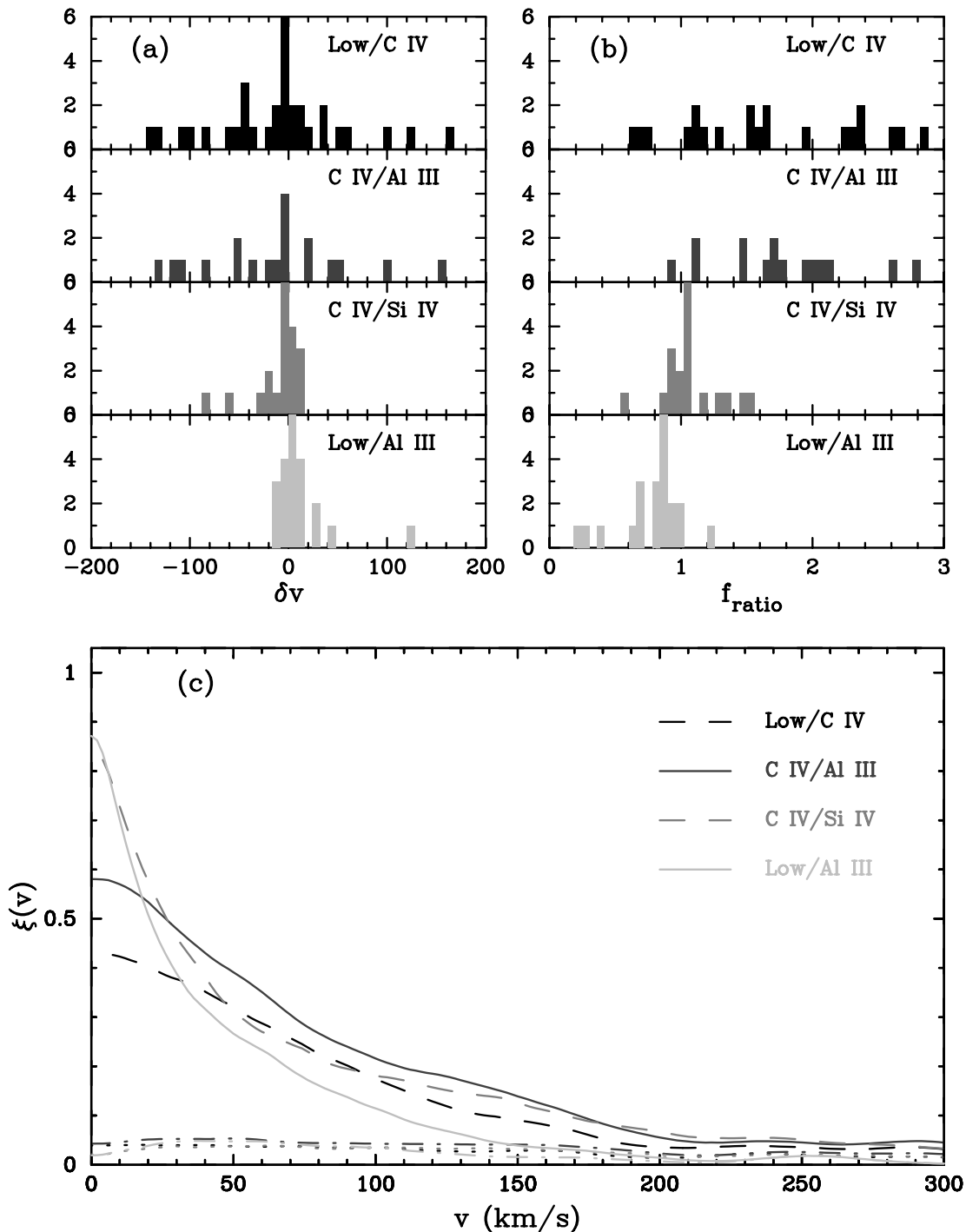


FIG. 7.—Empirical distributions of correlation test statistics (a) δv and (b) f_{ratio} , and (c) cross-correlation functions $\xi_{ab}(v)$ for low-ion vs. C IV (dark dashed curve), C IV vs. Al III (dark solid curve), C IV vs. Si IV (light dashed curve), and low-ion vs. Al III (light solid curve) velocity profiles. Lower dashed curves show 1σ errors.

As a result, disks with rotation speeds exceeding 150 km s^{-1} cannot be ruled out. In any case, the correlation between f_{edg} and Δv is tentative (see Fig. 9), and needs to be tested with larger data sets.

3.3. Cross-Correlation Functions

We next investigate whether the detailed component structures exhibited by the velocity profiles of various ions are correlated. In Figure 7c we plot $\xi_{ab}(v)$, the cross-

correlation functions between ions a and b , versus lag velocity, v , and the 1σ errors, $\sigma_{\xi_{ab}}(v)$. The $\xi_{ab}(v)$ are given by

$$\xi_{ab}(v) = \frac{1}{N} \sum_{k=1}^N \frac{1}{\sqrt{\xi_{aa}^k(0)\xi_{bb}^k(0)}} \sum_{i=1}^{n_k} [\tau_{ak}(u_i)][\tau_{bk}(u_i - v)], \quad (1)$$

where the first sum is over N profiles, and the second is over n_k velocity channels, u_i , spanning the k th absorption profile. The quantity $\tau_{ak}(v)$ is the optical-depth profile of ion a for the k th profile. The quantity $\xi_{aa}^k(0)$ is the autocorrelation

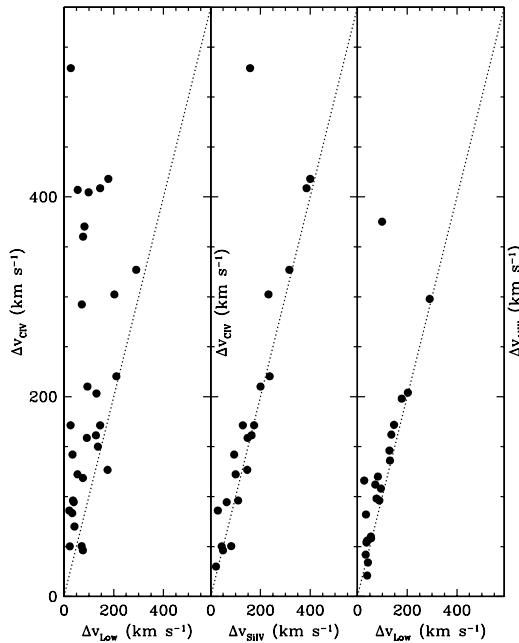


FIG. 8.—Plots of Δv for the ion pairs (a) C IV vs. low-ion, (b) C IV vs. Si IV, and (c) Al III vs. low-ion.

function for ion a in the k th profile at $v = 0$, and is defined as

$$\xi_{aa}^k(0) = \sum_{i=1}^{n_k} [\tau_{ak}(u_i)]^2. \quad (2)$$

As a result, the cross-correlation functions are normalized so that perfectly correlated ions yield $\xi_{ab}(v) = 1$ at zero lag velocity. The errors are dominated by cosmic variance and are computed by a “bootstrap” method (Efron & Tibshirani 1993).

Comparison between the cross-correlation functions and the errors demonstrates that in some cases, the measured $\xi_{ab}(v)$ are statistically significant out to $v \sim 150 \text{ km s}^{-1}$. The strongest correlations shown are between the low-ion and Al III profiles, and between the C IV and Si IV profiles. This confirms the rather accurate one-to-one alignment between the velocity components comprising these ion pairs (see

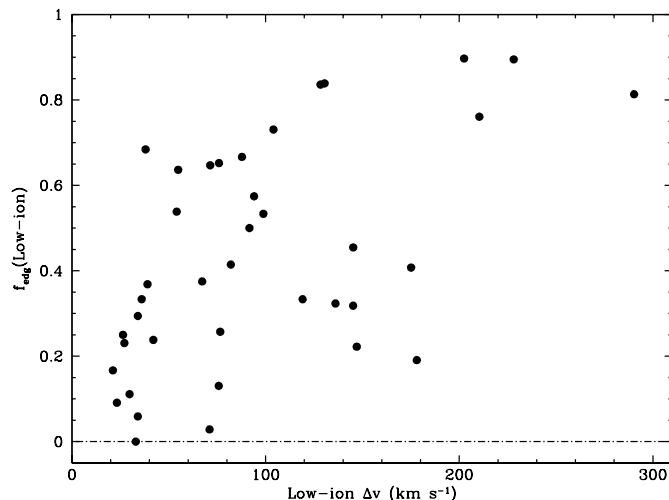


FIG. 9.—Plot of f_{cdg} vs. Δv for low-ion profiles in Table 1

Figs. 3 and 4). The 20 km s^{-1} half-width of ξ_{ab} for Al III versus low ion roughly equals the half widths of the wider components in Figure 3, which supports the idea of common velocity components for Al III and low ions. The 30 km s^{-1} half width of ξ_{ab} for C IV versus Si IV argues for common component structures for these two ions.

By contrast, the $\xi_{ab}(v)$ for the C IV versus low ions or C IV versus Al III exhibit significantly lower, but still statistically significant, values at $v = 0$ (the differences exceed 6σ). The lower $\xi_{ab}(0)$ stems from misalignment between the low-ion (or Al III) velocity components with the C IV components in many of the profiles. In this case, the correlation amplitude arises from overlap in velocity space between the ion pairs rather than one-to-one alignment between individual components. This interpretation is supported by the $\sim 80 \text{ km s}^{-1}$ half-widths of ξ_{ab} for the C IV versus Al III or C IV versus low-ion profiles. These half-widths more closely resemble the coherence scales of contiguous multiple components in the C IV profiles than the half-widths of individual components (see Fig. 1).

4. SUMMARY AND CONCLUDING REMARKS

Using high-resolution absorption spectra obtained with HIRES, the Echelle spectrograph on the Keck I telescope (Vogt 1994), we have probed the kinematics of ionized gas in a sample of 35 high-redshift damped $\text{Ly}\alpha$ protogalaxies. Specifically, we obtained velocity profiles of the high ions C IV and Si IV and the intermediate ion Al III. We studied the kinematic state of the gas by constructing empirical test statistics that characterize (1) the widths and symmetry properties of high-ion, intermediate-ion, and previously obtained low-ion velocity profiles, and (2) correlations between the kinematic properties of various ionic pairs.

What have we learned that is new? We answer this question by discussing model-independent conclusions inferred from the data.

1. The damped $\text{Ly}\alpha$ absorbers comprise distinct kinematic subsystems: a low-ion subsystem in which low ions such as Al II are physically associated with intermediate ions such as Al III, and a high-ion subsystem consisting of ions such as C IV and Si IV. This is indicated by the similarity between the C IV and Si IV velocity profiles and between the low-ion and Al III velocity profiles, and by the misalignment of the velocity components comprising the C IV and low-ion profiles.

2. The low-ion and high-ion kinematic subsystems are related despite misalignment of their velocity components. This follows from the detection of a statistically significant C IV versus low-ion cross-correlation function, which exhibits lower amplitude and a wider half-width than either the low-ion versus Al III or C IV versus Si IV cross correlation functions. Whereas the high cross-correlation amplitudes of the latter two ionic pairs arise from the coincidence between corresponding velocity components, the lower amplitude of the C IV versus low-ion cross-correlation function is due to a general overlap in velocity space between the line profiles. In any case, the relation between low-ion and high-ion subsystems is further indicated by a systematic effect in which $\Delta v_{\text{C IV}} \geq \Delta v_{\text{low}}$ in 29 out of 32 profiles.

3. The difference between the mean velocities of the C IV and Si IV velocity profiles or between the low-ion and Al III profiles exhibits distributions with dispersions equaling 23 and 30 km s^{-1} , respectively. By contrast, the low-ion versus

C IV distribution has a significantly wider dispersion of 67 km s^{-1} . This is more evidence for distinct kinematic subsystems.

4. The absence of intermediate ions and low ions from the high-ion subsystem indicates that the latter is optically thin at the Lyman limit. The lack of mixed ionization states distinguishes the high-ion gas in damped Ly α protogalaxies from high-ion gas in the ISM (Savage et al. 1993), high-redshift Lyman-limit systems (Prochaska 1999; Paper II), and $z \sim 0.7$ Mg II-selected absorbers (Churchill et al. 1999), where the velocity profiles of the low and intermediate ions resemble those of the high ions.

These results have rather general implications. First, kinematic subsystems placed in the same potential well generate velocity profiles that tend to overlap in velocity space. In cases where the velocity field of the neutral gas is constrained to fewer degrees of freedom than the ionized gas, the resulting profiles will be characterized by $\Delta v_{\text{C IV}} \geq \Delta v_{\text{low}}$. Therefore, in Paper II we will test the hypothesis that both kinematic subsystems are subjected to gravitational forces

arising from the same mass distribution. Second, the absence of ionized gas optically thick at the Lyman limit implies a distinction between the damped Ly α systems on the one hand and the Lyman-limit systems and Mg II absorbers on the other. This is potentially significant, because most models assume that both classes of absorber arise in the same physical object. Finally, in Paper II we use the empirical distributions of test statistics as well as the empirical C IV versus low-ion cross-correlation function to constrain semianalytic models of galaxy formation. Specifically, we focus on models in which ionized gas in virialized dark matter halos falls onto centrifugally supported neutral hydrogen disks.

We wish to thank Eric Gawiser and David Tytler for valuable discussions. We also thank Wal Sargent for generously giving us data prior to publication. A. M. W. was partially supported by NSF grant AST 00-71257, and J. X. P. acknowledges support from a Carnegie postdoctoral fellowship.

REFERENCES

- Churchill, C. C., Mellon, R. R., Charlton, J. C., Jannuzi, B. T., Kirhakos, S., Steidel, C. C., & Schneider, D. P. 1999, *ApJ*, 519, 43L
 Efron, B., & Tibshirani, R. J. 1993, *An Introduction to the Bootstrap* (New York: Chapman & Hall)
 Frodesen, A. G., Skjeggstad, O., & Tofte, H. 1979, *Probability and Statistics in Particle Physics* (Bergen: Universitetsforlaget)
 Haehnelt, M. G., Steinmetz, M., & Rauch, M. 1998, *ApJ*, 495, 647
 Jedamzik, K., & Prochaska, J. X. 1998, *MNRAS*, 296, 430
 Kauffmann, G. 1996, *MNRAS*, 281, 475
 Ledoux, C., Petitjean, P., Bergeron, J., Wampler, E. J., & Srianand, R. 1998, *A&A*, 337, 51
 Mo, H. J., & Miralda-Escudé, J. 1996, *ApJ*, 469, 589 (MM)
 Prochaska, J. X. 1999, *ApJ*, 511, L71
 Prochaska, J. X., & Wolfe, A. M. 1996, *ApJ*, 470, 403
 ———. 1997, *ApJ*, 487, 73 (PW97)
 ———. 1998, *ApJ*, 507, 113 (PW98)
 Savage, B. D., Lu, L., Weymann, R. J., Morris, S. L., & Gilliland, R. L. 1993, *ApJ*, 404, 124
 Vogt, S. S., et al. 1994, *Proc. SPIE*, 2198, 362
 Wolfe, A. M. 1995, in *ESO Workshop on QSO Absorption Lines*, ed. G. Meylan (Berlin: Springer), 13
 ———. 1997, in *Critical Dialogues in Cosmology*, ed. N. Turok (Singapore: World Scientific), 500
 Wolfe, A. M., & Prochaska, J. X. 2000, *ApJ*, 545, this issue (Paper II)